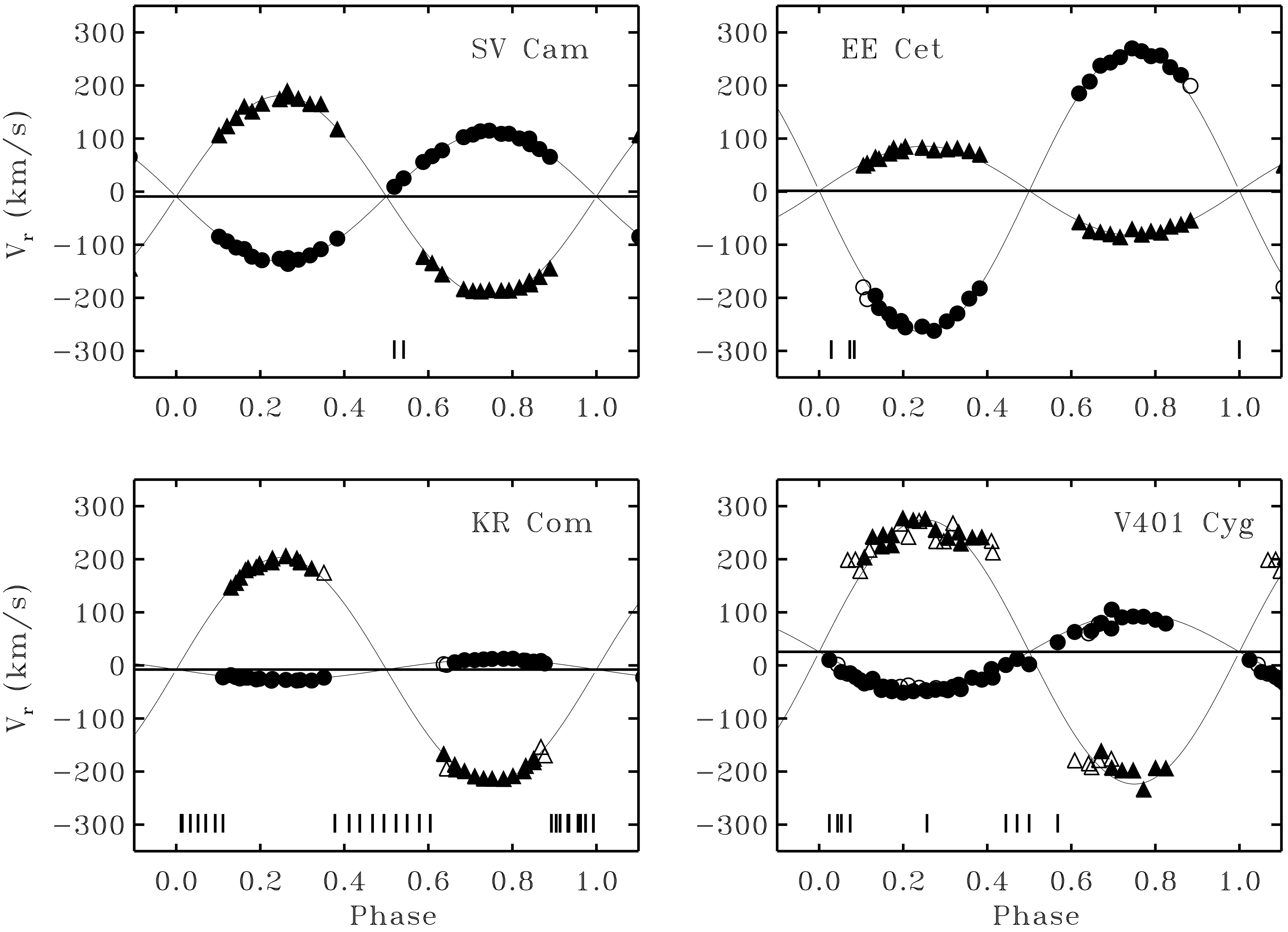
SV Cam
EE Cet
KR Com
V401 Cyg
V_r (km/s)
V_r (km/s)
300
200
100
0
−100
−200
−300
0.0
0.2
0.4
0.6
0.8
1.0
Phase
Phase

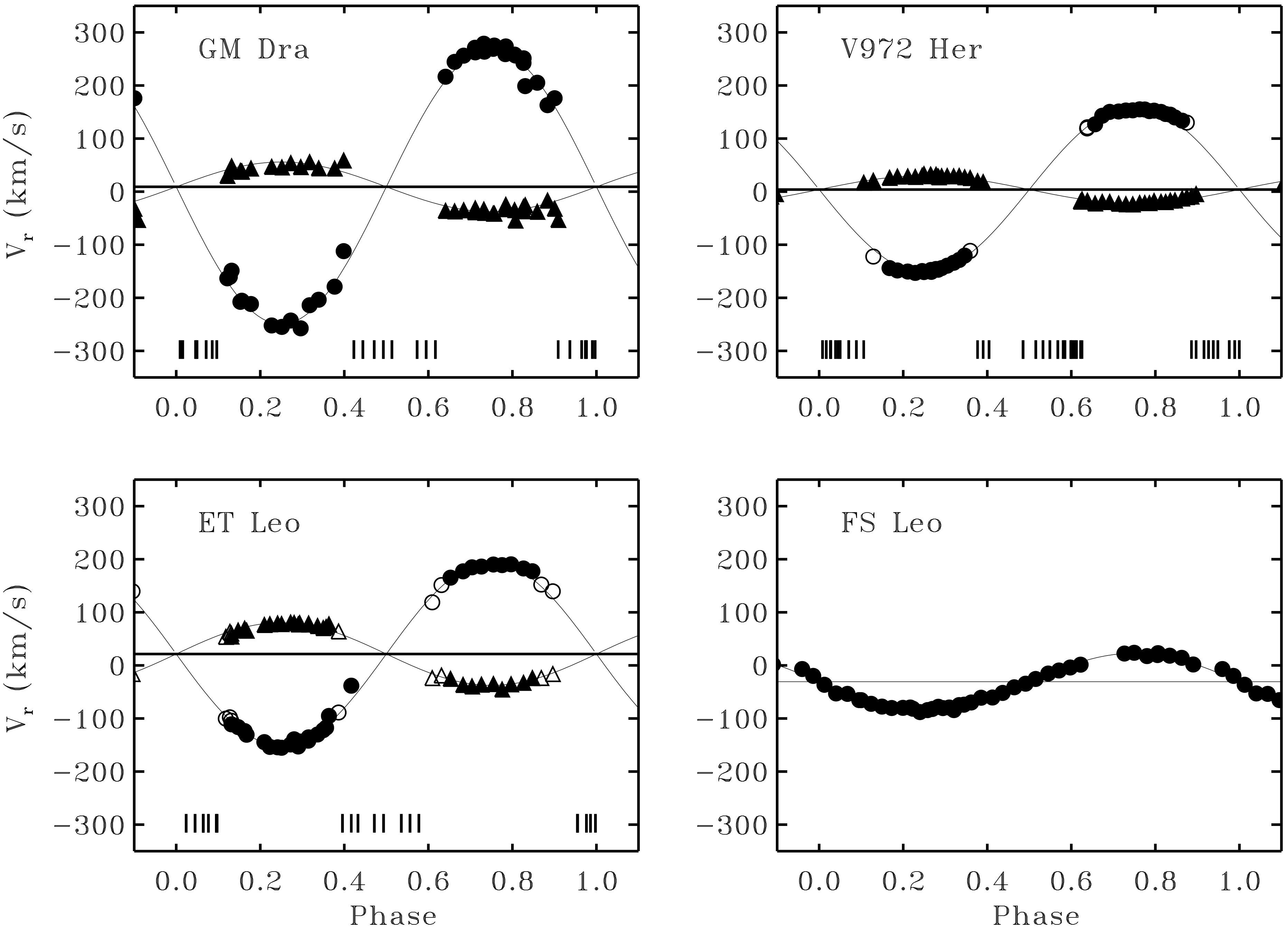
GM Dra
V972 Her
ET Leo
FS Leo
V_r (km/s)
V_r (km/s)
300
200
100
0
−100
−200
−300
0.0
0.2
0.4
0.6
0.8
1.0
Phase
Phase

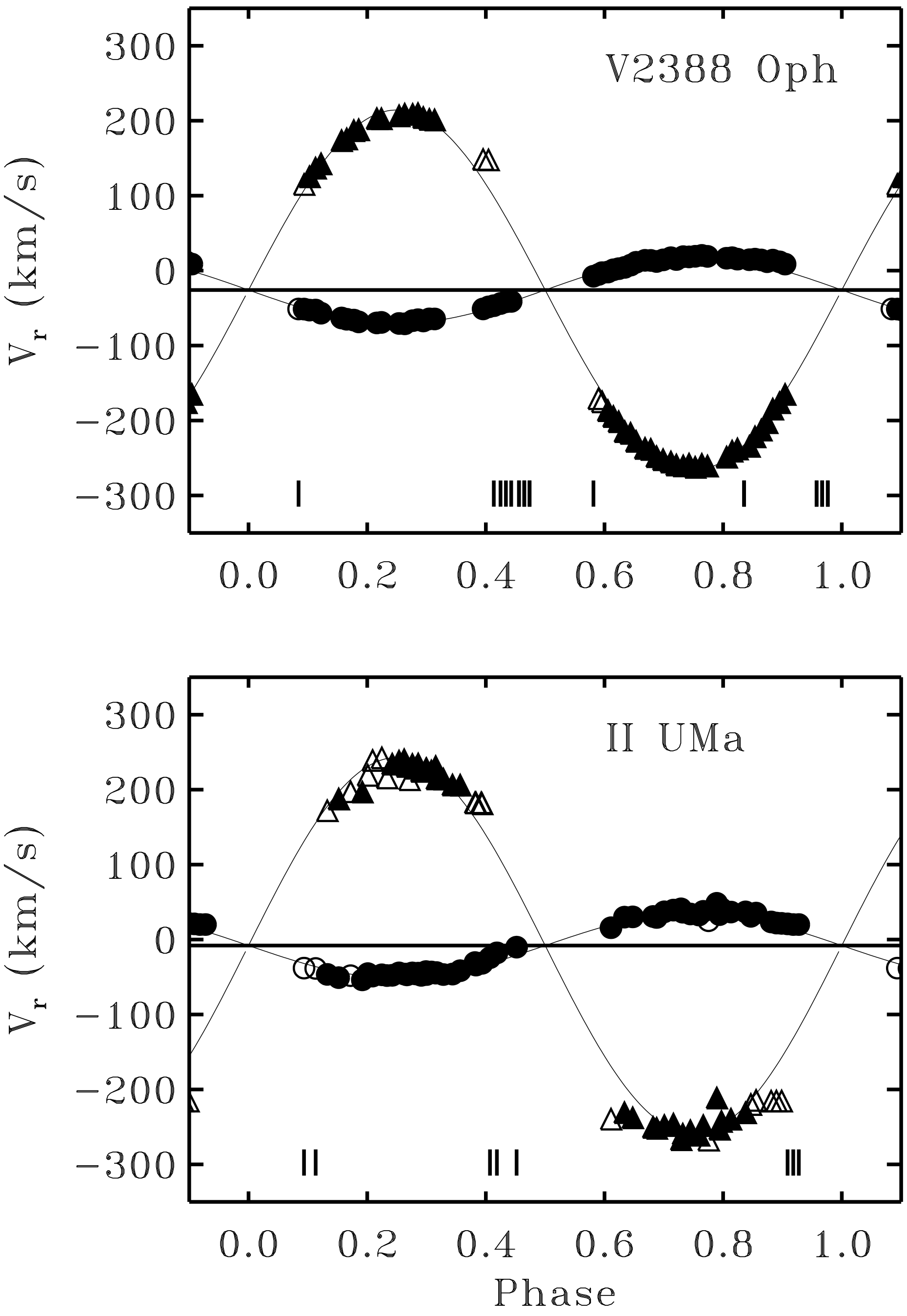
V2388 Oph
II UMa
V_r (km/s)
V_r (km/s)
300
200
100
0
−100
−200
−300
0.0
0.2
0.4
0.6
0.8
1.0
Phase

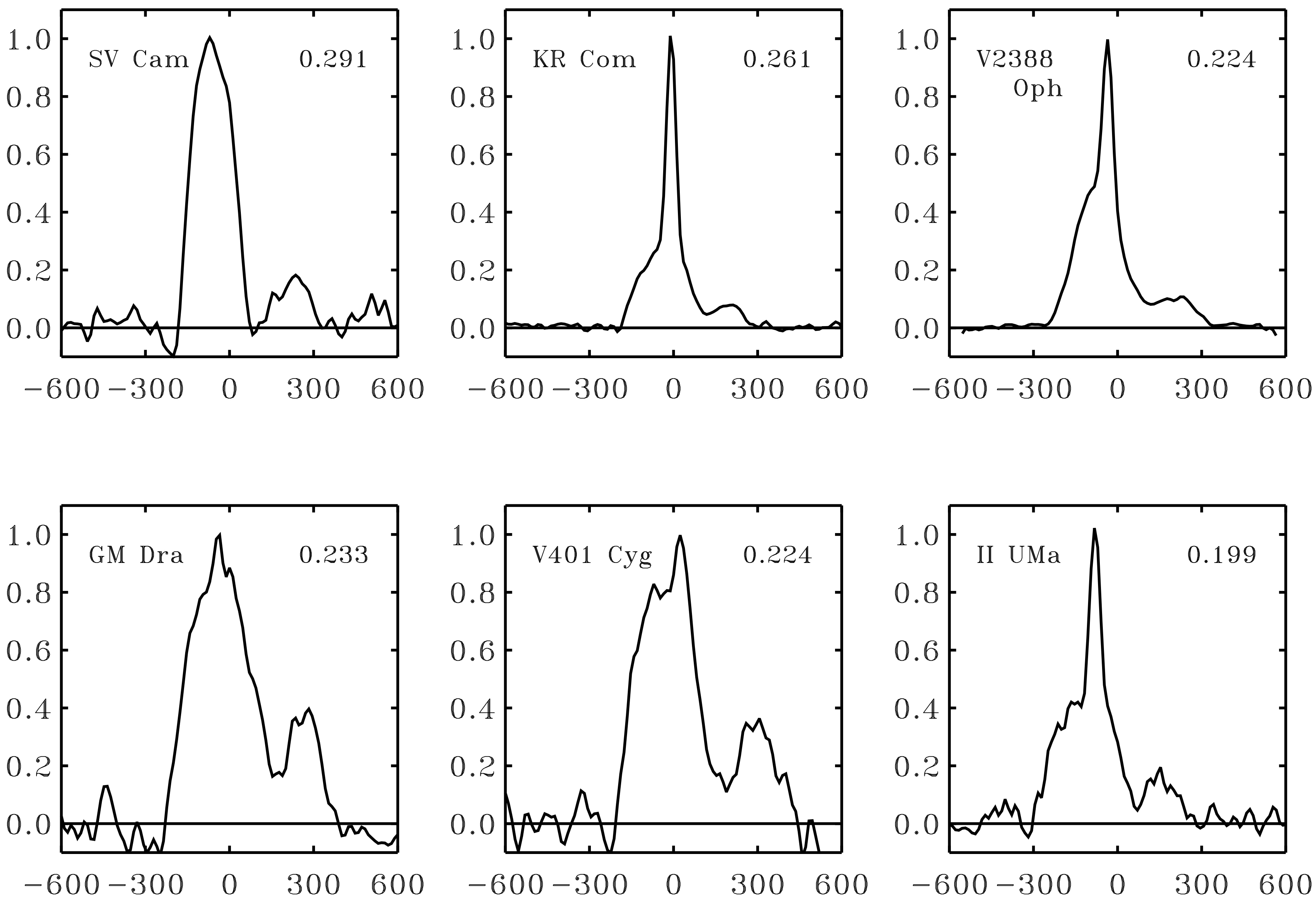
SV Cam
0.291
KR Com
0.261
V2388
Oph
0.224
GM Dra
0.233
V401 Cyg
0.224
II UMa
0.199
1.0
0.8
0.6
0.4
0.2
0.0
−600
−300
0
300
600

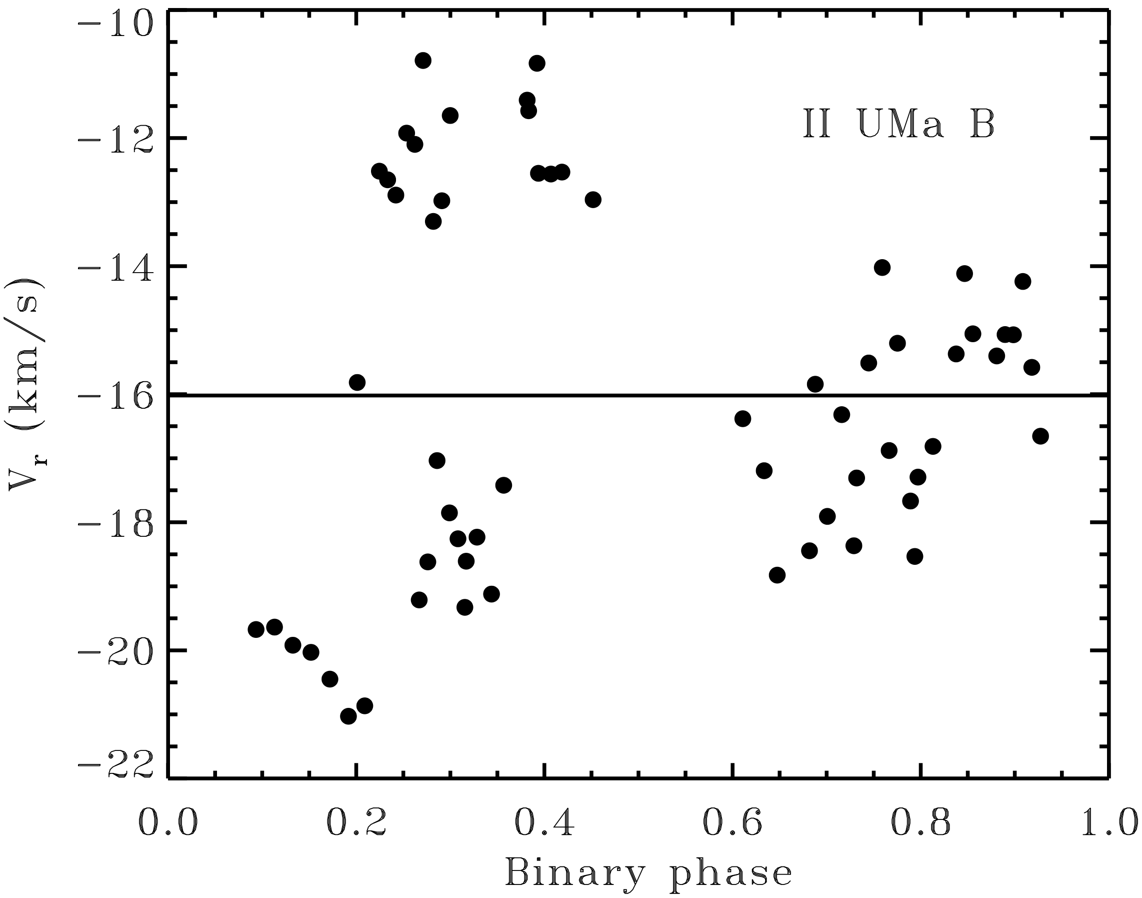
II UMa B
V_r (km/s)
−10
−12
−14
−16
−18
−20
−22
0.0
0.2
0.4
0.6
0.8
1.0
Binary phase

arXiv:astro-ph/0201213v2 29 May 2002

Radial Velocity Studies of Close Binary Stars. VI[1]

Slavek M. Rucinski, Wenxian Lu,[2] Christopher C. Capobianco,
Stefan W. Mochnacki, R. Melvin Blake, J. R. Thomson

David Dunlap Observatory, University of Toronto
P.O.Box 360, Richmond Hill, Ontario, Canada L4C 4Y6

`rucinski,lu,capobian,mochnacki,blake,jthomson@astro.utoronto.ca`

and

Waldemar Ogłoza, Greg Stachowski

Mt. Suhora Observatory of the Pedagogical University
ul. Podchorażych 2, 30-084 Cracow, Poland

`ogloza,stachowski@ap.krakow.pl`

ABSTRACT

Radial-velocity measurements and sine-curve fits to the orbital velocity variations are presented for the sixth set of ten close binary systems: SV Cam, EE Cet, KR Com, V410 Cyg, GM Dra, V972 Her, ET Leo, FS Leo, V2388 Oph, II UMa. All systems except FS Leo are double-lined spectroscopic binaries. The type of FS Leo is unknown while SV Cam is a close, detached binary; all remaining systems are contact binaries. Eight binaries (all except SV Cam and V401 Cyg) are the recent photometric discoveries of the Hipparcos satellite project. Five systems, EE Cet, KR Com, V401 Cyg, V2388 Oph, II UMa, are members of visual/spectroscopic triple systems. We were able to observe EE Cet separate from its companion, but in the remaining four triple systems we could separate the spectral components only through the use of the broadening-function approach. Several of the studied systems are prime candidates for combined light and radial-velocity synthesis solutions.

Subject headings: stars: close binaries - stars: eclipsing binaries – stars: variable stars

---

[1] Based on the data obtained at the David Dunlap Observatory, University of Toronto.

[2] Current address: NASA/GSFC, Bldg. 26, 8800 Greenbelt Road, Greenbelt, MD 20771

1. INTRODUCTION

This paper is a continuation in a series of papers of radial-velocity studies of close binary stars: Lu & Rucinski (1999, Paper I), Rucinski & Lu (1999, Paper II) and Rucinski et al. (2000, Paper III), Lu et al. (2001, Paper IV), Rucinski et al. (2001, Paper V). The main goals and motivations are described in these papers. The companion paper of Rucinski (2002, Paper VII) describes the technical details and methods of data reductions as well as the resulting measurement uncertainties, based on data in the six previous papers.

This paper is structured in the same way as Papers I – V in that most of the data for the observed binaries are in two tables consisting of the radial-velocity measurements (Table 1) and their sine-curve solutions (Table 2). Section 2 of the paper contains brief summaries of previous studies for individual systems. Figures 1 – 3 show the data and the radial velocity solutions.

The observations reported in this paper have been collected between October 1997 and June 2001; the ranges of dates for individual systems can be found in Table 1. All systems discussed in this paper, except SV Cen, have been observed for radial-velocity variations for the first time. We have derived the radial velocities in the same way as described in previous papers. See Paper IV and Paper VII for discussion of the broadening-function approach used in the derivation of the radial-velocity orbit parameters: the amplitudes, K_i, the center-of-mass velocity, V_0, and the time-of-eclipse epoch, T_0.

The data in Table 2 are organized in the same manner as in previous papers. In addition to the parameters of spectroscopic orbits, the table provides information about the relation between the spectroscopically observed epoch of the primary-eclipse T_0 and the recent photometric determinations in the form of the (O–C) deviations for the number of elapsed periods E. It also contains our new spectral classifications of the program objects.

For further technical details and conventions used in the paper, please refer to Papers I – V and VII of this series.

2. RESULTS FOR INDIVIDUAL SYSTEMS

2.1. SV Cam

SV Cam is a short-period, detached binary system. It has been the subject of numerous photometric and four spectroscopic studies. In two first spectroscopic investigations, Hiltner (1953) and Rainger et al. (1991), the system was observed as a single-lined spectroscopic binary (SB1). The secondary component was subsequently detected by Pojmanski (1998) who used the spectral resolution three times lower than ours. Oezeren et al. (2001) observed the system at a relatively high spectral resolution, but chose to adopt the spectroscopic results of Pojmanski (1998), concentrating on the details of line-profile changes, in relation to the known, high activity of this short-period

RS CVn-type system.

Our double-lined (SB2) spectroscopic orbit is very well defined, with small errors of the orbital parameters. We note that determinations of the radial velocity semi-amplitude of the primary component, K_1, agree well in the four existing solutions. Starting with Hiltner (1953) (as reanalyzed by Rainger et al. (1991)), Rainger et al. (1991), Pojmanski (1998) and the current, the results have been (in km s^{-1}) : 121.7 ± 1.9, 122.3 ± 1.5, 118.5 ± 2.0, and 121.86 ± 0.76. The results of Pojmanski (1998) differ the most, but are still within the errors of the solutions. The center of mass velocity, V_0, seems to show a secular progression, although the data of Pojmanski (1998) deviate from the trend. In the same order as before: -16.2 ± 1.4, -11.2 ± 1.2, -13.7 ± 1.5 and -9.13 ± 0.78 km s^{-1}. Noting that the observations were made in 1947, 1988, 1993 and 1997, the trend may be related to the motion about the third body with the period of about 65 – 75 years and the semi-amplitude of about 2 km s^{-1} (Rainger et al. 1991).

The results of Pojmanski (1998), although the first to reveal the motion of the secondary component, show deviations described above and, even more importantly, differ rather substantially from our results in the value of K_2: 211.5 ± 5.5 versus our 190.17 ± 1.73 km s^{-1}. Possibly, the discrepancies are due to the rather complex reduction scheme of the previous study which involved successive removal of the two spectral signatures from individual spectra. This was entirely unnecessary in our case because the broadening functions that we analyzed were very well defined and radial velocities of both components could be measured with great ease. Figure 4 shows one of the broadening functions for SV Cam, in comparison with other systems analyzed in this paper. On the basis of the widths of the individual signatures in the broadening functions, and taking into consideration the instrumental broadening, we estimate the apparent rotation velocity of the components, $V_1 \sin i = 122 \pm 10$ km s^{-1} and $V_2 \sin i = 85 \pm 8$ km s^{-1}. Patkos & Hempelman (1994) found that the orbit of SV Cam is oriented exactly edge on, $i \simeq 90°$, so that these are our estimates of the equatorial rotational velocities. We note that Pojmanski (1998) estimated $V_1 \sin i = 105$ km s^{-1} while a solar-size star in the orbital synchronism would have $V \sin i \simeq 90$ km s^{-1}.

The total mass, $(M_1 + M_2) \sin^3 i = 1.871 \pm 0.045 \, M_\odot$, and the mass ratio, $q = 0.641 \pm 0.007$, lead to the masses, 1.14 and 0.73 $M_\odot$, which are somewhat large for the combined spectral type that we estimated as G2V, but would agree with the estimate of Pojmanski (1998) of F8V. The estimated value of $V_1 \sin i$ would also suggest a primary larger than the Sun. The mean color index from the Tycho-2 Catalog (Hog et al. 2000, TYC2), $B - V = 0.62$, is in agreement with our spectral type. We should note that our low-dispersion classification as well as the TYC2 color index relate to the combined photometric properties of the system.

The ephemeris that we used was that of the photometric study of Pribulla et al. (2001) which covered the time range actually slightly after our observations and gave a perfect agreement for the time of eclipses. Since the published T_0 was already shifted from the actual time of observations, we recalculated the published moment to our T_0 so that no whole cycles appear in the phase count in Table 2. We also used the orbital period from the same study simplifying it to the six decimal places, 0.593073 days, which was entirely sufficient for the duration of our observations. We note that the orbital period cited in the Hipparcos Catalogue (ESA 1997, HIP) was slightly different, 0.593075 days, while Pojmanski (1998) used 0.593071 days.

With a good Hipparcos parallax, $p = 11.77 \pm 1.07$ mas (HIP), and well determined tangential motions, $\mu_\alpha \cos\delta = 41.5 \pm 1.1$ mas/y and $\mu_\delta = -150.9 \pm 1.1$ mas/y (TYC2), the system of SV Cam appears to be one of the best currently characterized close binary systems on the lower main sequence. Of note is the relatively large spatial motion of 64 km s^{-1}, mostly the result of the large tangential motion; the systemic radial velocity is moderate, $V_0 = -9.13 \pm 0.78$ km s^{-1}.

2.2. EE Cet

Variability of the combined light of the visual binary ADS 2163 was discovered by the Hipparcos satellite mission (ESA 1997). The light curve was relatively sparsely covered, showing variation of about 0.23 magnitude. On the basis of an observation that the southern component rotates too rapidly for the technique used by Nordstroem et al. (1997) to measure its radial velocity, this component was our prime candidate for being the source of the variability observed by Hipparcos. We could observe this star without contamination by the northern companion which is separated by 5.6 arcsec. We found that the southern component is a contact binary system and we assume that it should carry the variable-star name EE Cet. It appears to be a contact system of the W-type, i.e. with the less massive component eclipsed during the primary eclipse; however, it is the more massive, slightly cooler component which gives a better defined signature in the broadening function, probably because of its larger radiating area. In phasing our observations, we used the HIP prediction for times of eclipses.

We caution that there exists certain confusion in the literature as to which component of ADS 2163 should be called A and which B. On the average, the southern component, which we identify here with EE Cet, is the fainter of the two and this agrees with the naming of the stars in the HIP catalog, where the visual binary appears under CCDM J02499+0856. However, in the ADS catalog the names are actually reversed and in SIMBAD it is the northern, brighter component which carries the name of EE Cet. Lampens et al. (2001) published photometric data for one epoch and give $V(A) = 9.47$ and $V(B) = 9.83$ identifying the southern component as fainter. To complicate things even further, we found that the northern component of ADS 2163 is also a close binary system showing radial velocity variations; this component may very well be a variable star. However, currently we have insufficient radial-velocity data to analyze this binary system; we hope to be able to provide such data in one of the subsequent papers of this series. We only note that Nordstroem et al. (1997) gave its radial velocity, $V_0 = +2.26 \pm 0.04$ km s^{-1}, which is similar to the center-of-mass velocity of EE Cet, $V_0 = +1.60 \pm 0.93$ km s^{-1}.

The radial velocity solution for EE Cet is very well defined. However, because of the lack of reliable Hipparcos parallax (it is actually listed as negative), we cannot derive the absolute magnitude of the binary. Once the two components of the visual binary are photometrically separated and parallaxes for both components determined, this quadruple system may turn out as one of the most interesting among bright stars of the sky.

2.3. KR Com

KR Com is another Hipparcos satellite photometric discovery. In phasing our observations, we used the HIP prediction for times of minima. The shallow eclipses are of almost identical depth of only about 0.06 mag. so there is no obvious reason for the EB classification which has been used in the HIP Catalog; the system is a contact binary and would normally be designated as EW.

The star had been known as a very close visual system of very small mean separation of only 0.12 arcsec. In the HIP catalog it appears as CCDM J13203+1746, with the magnitude difference of components of 0.60 magnitude; it is also known as ADS 8863. The visual binary was a subject of numerous speckle interferometry investigations. While these observations are of lesser relevance in the context of this paper, we note that the close binary shows rather large radial-velocity variations, so that its small photometric variation may be partly due to "dilution" of the close-binary variability signal in the combined light of the visual system. Our broadening function indicates that the brighter component is the contact system while the fainter component is a slowly-rotating star, as can be seen in Figure 4. The brightness of the visual companion is large, $L_3/(L_1+L_2) = 0.56 \pm 0.04$ (at light maxima of the close binary), which confirms the previous magnitude-difference estimates.

Our radial velocity orbit is very well defined, mostly due to the brightness of the system at $V_{max} = 7.14$. We could very well isolate the signature of the third, slowly-rotating star, as one can see in Figure 4. Allowing for the contribution of the visual companion, and with the Hipparcos parallax of $p = 13.07 \pm 0.87$ mas, one obtains $M_V^{tot} = 2.72 \pm 0.15$ and thus $M_V^{EW} = 3.20$, while the RD97 calibration predicts $M_V^{EW}(cal) = 3.42$. The latter is obtained using the color TYC2 index, $(B-V) = 0.52$, which suggests a spectral type of about F8; our direct classification is G0IV, although the spectral type and the luminosity class relate to the combined properties of the triple system. The average radial velocity of the third component, $\overline{V_3} = -3.59 \pm 0.12$ km s^{-1} (the error of a single observation is 0.93 km s^{-1}), is significantly different from the center-of-mass velocity of the binary, $V_0 = -7.86 \pm 0.38$ km s^{-1}.

KR Com has one of the smallest mass ratios known among contact binaries, $q = 0.091 \pm 0.002$. The total minimum mass, $(M_1 + M_2)\sin^3 i = 0.517 \pm 0.008\,M_\odot$, indicates that the orbit is rather strongly inclined to the line of sight, which is another reason for the small photometric amplitude. As is normally observed, the small mass ratio is associated with the A-type characteristics of the contact system, i.e. the deeper eclipse corresponds to the more massive star being eclipsed by the less massive companion.

2.4. V401 Cyg

Together with SV Cam, this binary is one of two in this paper which had not been discovered by the Hipparcos mission. In fact it was discovered by Hoffmeister (1929) and since then was sporadically observed, mostly for eclipse timing. Photometrically, the binary appears to be a rather typical contact system with relatively large light variation of about 0.55 magnitude. Herzeg (1993) pointed out that the orbital period of the system is lengthening. Wolf et al. (2000) conducted a light-curve analysis and found the best-fitting, photometric mass ratio, $q_{ph} \simeq 0.3$. To some extent to our surprise (because we see so many cases of $q_{ph} \neq q_{sp}$), we found $q = 0.290 \pm 0.011$.

Our radial velocity orbit was based on the assumed period of 0.582714 days, as in the HIP Catalog. For the initial time of the primary minimum, we used the data in Nelson (2001) obtained during the span of our observations. The agreement is very good (see Table 2) given the somewhat larger error of our T_0 for this star, when compared with other binaries. The main reason for the larger error was the relative faintness of this binary ($V_{max} \simeq 10.5$) and the fact that we discovered a third "light" in the system. The spectral signature of the third star (which may, but does not have to be physically associated with the binary) can be seen in the broadening function in Figure 4 as a small feature projecting onto the prominent signature of the primary component. Similar noise fluctuations are common in broadening functions of faint stars, but this one is always present, at the same radial velocity at all orbital phases. By integrating the amount of light in this additional feature, we could estimate that, at the light maximum of the binary, $L_3/(L_1 + L_2) = 0.03 \pm 0.01$. Because the third-light contribution is so small, we neglected it in our measurement. However, it may have slightly affected the amplitude of the primary component, K_1, due to the fact that (1) the radial velocities of primary component are, by necessity, always close to V_0 and (2) the third component appears to have a very small radial velocity relative to the binary system.

2.5. GM Dra

GM Dra was discovered photometrically by the Hipparcos satellite as a 9th magnitude contact binary with a fairly large variation of about 0.27 mag. The system was observed photometrically by Çiçek et al. (2001), one year after our observations. The authors gave a recent moment of the light minimum and improved the value of the orbital period.

Our radial velocity orbit is quite well defined (Figure 2). GM Dra is a rather uncomplicated contact system of the W-type, i.e. with the smaller star eclipsed during the deeper minimum (although the difference in the depth of the eclipses is very small). The spectral type F5V and the color index $B - V = 0.48$ agree. The absolute magnitude derived from the HIP parallax, $p = 10.16 \pm 0.88$ mas and $V_{max} = 8.65$ is $M_V = 3.68 \pm 0.20$, which is in perfect agreement with the calibration of Rucinski & Duerbeck (1997, RD97), $M_V(cal) = 3.66$.

2.6. V972 Her

V972 Her is another Hipparcos photometric discovery. The light variation is small, about 0.08 mag. indicating a small orbital inclination or “dilution” of light in a triple system. The HIP light curve is very well defined and suggests a perfect contact system (EW). It is not clear why the system was given there a classification EB which would suggest unequally deep minima.

Our radial velocity orbit is very well defined, mostly thanks to the large brightness of the system, $V_{max} = 6.62$. With the relatively large HIP parallax (the largest in this group of binaries), $p = 16.25 \pm 0.61$ mas, and thus $M_V = 2.67 \pm 0.09$, the system is the nearest contact binary in this group of ten binary systems. The RD97 calibration with $B - V = 0.39$ (which agrees with our spectral type F4V) gives $M_V(cal) = 2.87$, which is in marginal agreement with the directly determined M_V. The very small value of $(M_1 + M_2) \sin^3 i = 0.276 \pm 0.006\, M_\odot$ confirms the expectation of a very small orbital inclination angle.

Our initial T_0 was based on the time determined by Keskin et al. (2000) which was obtained in the middle of our spectroscopic run, but gives a rather large O–C = +0.0224 days. We have no explanation for this discrepancy because our T_0 is nominally accurate to 0.0016 days. The binary is a contact system of the W-type with the less massive component eclipsed at the deeper minimum; however, the difference in depth is very small.

2.7. ET Leo

The photometric variability of the star was discovered by the Hipparcos mission. The period assigned there was equal to one half of the true orbital period. Instead of the exact double of the HIP period, we used the value given by Gomez–Forrellad et al. (1999) of 0.346503 days. Their initial epoch T_0 (obtained three years before our observations) and the new period predict the moment of the deeper eclipse which agrees well with our determination (see Table 2).

Our spectral type, G8V, appears to be late relative to the TYC2 color index $(B - V) = 0.61$. The parallax is large, $p = 13.90 \pm 1.44$ mas, but apparent magnitude is only moderate, $V_{max} = 9.48$, indicating that the system is intrinsically rather faint: $M_V = 5.20 \pm 0.24$. The RD97 calibration, utilizing the $(B - V)$ index as above, predicts $M_V(cal) = 4.01$; an agreement in M_V would require a color index as large as $(B - V) \simeq 1.0$. This discrepancy between the spectral type and the color index remains to be explained.

ET Leo must be observed at a relatively low orbital inclination angle. This would explain the small photometric variability of only 0.06 mag. as well as the small radial-velocity amplitudes leading to $(M_1 + M_2) \sin^3 i = 0.450 \pm 0.012\, M_\odot$.

2.8. FS Leo

The photometric variability of FS Leo was discovered by the Hipparcos mission. In spite of our efforts, we have not been able to find any spectral signatures of the secondary component in the system, so that this is a single-lined binary (SB1); it is the only such system in this group of ten binary systems. The radial velocity of the only visible component is very well defined. For the initial phasing of our observations, we used the original HIP prediction which gave a time deviation O–C = -0.035 days.

Our spectral type is F2V and the photometric data derived from the HIP and TYC databases give $V_{max} = 8.94$ and $(B - V) = 0.26$, the latter suggesting a slightly earlier spectral type around F0. The HIP parallax, $p = 6.12 \pm 1.41$ leads to $M_V = 2.87 \pm 0.51$. At this point we are unable to classify the system, but it is unlikely that this is a contact system. Of interest is the large spatial velocity of the system of 70 km s^{-1} which results mostly from the large tangential motion: 71.3 ± 1.1 and -38.7 ± 1.1 mas/year in both coordinates (TYC2).

2.9. V2388 Oph

This bright, 6th magnitude, very close visual binary (Fin 381, CCDM J17542+1108) has been the subject of many speckle interferometry investigations. The study of Soederhjelm (1999) resulted in the following set of the parameters: the separation, $a = 0.088$ arsec, the magnitude difference between components, $\Delta m = 1.80$ mag, the mean HIP magnitude for the primary $H_p = 6.45$, the orbital period, $P = 8.9$ years. Δm derived in this study was much larger than in several previous speckle interferometry investigations which usually suggested a number around 0.2 mag. We note that our entirely independent derivation based on the broadening functions gives $L_3/(L_1 + L2) = 0.20 \pm 0.02$, hence $\Delta m = 1.75 \pm 0.02$ mag., confirming the result of Soederhjelm (1999).

Rodriguez et al. (1998) discovered variability of the star, apparently independently of the HIP discovery. They classified it as a W UMa-type system with a relatively long orbital period of 0.802 days. Newer photometry of Yakut & Ibanoglu (2000) (used for T_0 in Table 2) confirmed that the HIP times-of-minima prediction; in fact, the HIP ephemeris gives a slightly smaller O–C for the time of the primary eclipse. The *ubvy* photometric data agree with the previous spectral type of F5Vn assuming no interstellar reddening. We would tend to give the star a slightly earlier spectral type, F3V. The HIP light curve is very well defined, and has a shape typical for a contact system, with eclipses 0.30 and 0.25 mag. deep. The relatively large HIP parallax, $p = 14.72 \pm 0.81$, and $V_{max} = 6.13$, gives $M_V = 1.97 \pm 0.13$ for the whole triple system hence $M_V^{EW} \simeq 2.17$, while the RD97 calibration predicts $M_V(cal) = 1.78$ for the W UMa-type binary, assuming $(B - V)_0 = 0.41$ from TYC2. The system appears to be one of the most luminous among currently known contact binaries. This may explain the imperfect agreement in M_V at the high-luminosity end where the RD97 calibration becomes highly uncertain.

As for other triple-lined systems, we measured the radial velocities of the binary after removing the third-body signature from the broadening function first and then by analyzing the remaining contact-binary BF. The radial velocity orbit of the close binary is very well defined (Figure 3) and describes a typical A-type contact system with moderately small mass-ratio, $q = 0.186 \pm 0.002$. The minimum mass, $(M_1 + M_2)\sin^3 i = 1.93 \pm 0.03\, M_\odot$, when related to the spectral type of about F3–F5, suggests a rather large orbital inclination angle, $i \simeq 90^\circ$. Thus, in spite of the necessity of dealing with a complicated BF (Figure 4), the radial-velocity parameters for V2388 Oph are very well defined.

The radial velocity measurements for the third component show some residual dependence on the phase of the close binary which may indicate some "cross-talk" in the measurements; we illustrate a similar, but larger effect in the case of the next system, II UMa. The semi-amplitude of the variations which correlate with the binary phase is about 2.5 km s^{-1}, which leads to a slightly elevated error per a single-observation of 1.50 km s^{-1}; for a single sharp-line star we could expect an error at the level of $1.2 - 1.3$ km s^{-1} or less. The mean radial velocity of the third component, $\overline{V_3} = -30.64 \pm 0.20$ km s^{-1}, is significantly different from the center-of-mass velocity for the binary, $V_0 = -25.88 \pm 0.52$ km s^{-1} which may result from the motion on the 8.9-year orbit.

2.10. II UMa

The photometric variability of the star was discovered by the Hipparcos satellite. The HIP prediction on the time-of-eclipse served very well for phasing of our observations. The star is a known, close visual binary, designated as ADS 8594 or CCDM J12329+5448, with the separation of component of 0.87 arcsec and difference in brightness 1.64 mag.

The broadening functions (see Figure 4) show a well-defined signature of the third component with the relative brightness, $L_3/(L_1 + L_2) = 0.17 \pm 0.01$, implying $\Delta m = 1.92 \pm 0.01$ mag. The triple-star characteristics of the star were handled by us in the same way as for the previously described star, V2388 Oph. Again, we see some unwelcome cross-talk in the radial velocities V_3, as shown in the plot versus the close-binary phase in Figure 5. This case is a bit more extreme than for V2388 Oph, with the error per single observation of 2.86 km s^{-1} in place of the expected $1.2 - 1.3$ km s^{-1} or less. We do not have a ready explanation for the coupling between the velocities and why the scatter appears to be increased only within the first half of the orbit. The dependence of V_3 on the binary-system phase has been observed in some triple stars in our program, but we usually have no simple explanation for its occurrence. However, we are not very concerned about its presence because our goal is the radial velocity orbit of the close binary system, which is in fact very well defined (see Figure 3). The average velocity of the third component, $\overline{V_3} = -16.02 \pm 0.37$ km s^{-1}, can be compared with the center-of-mass velocity of the close binary, $V_0 = -8.02 \pm 1.10$ km s^{-1}.

The binary is a long-period ($P = 0.825$ days) contact system of the A-type. Our spectral type suggests elevated luminosity, F5III, but classification of strongly broadened spectra of contact binaries is not easy, especially when combined with the spectrum of the third component. However, a high luminosity would agree with the relatively large size of the system implied by the long orbital period. The system is quite distant, because its HIP parallax is $p = 5.04 \pm 1.81$ mas. With the observed $V_{max} = 8.14$ for the whole system, $M_V = 1.65 \pm 0.8$. Using $L_3/(L_1 + L2) = 0.17 \pm 0.01$, the absolute magnitude of the close binary is $M_V^{EW} = 1.82$, which agrees rather well with the RD97 calibration predicting $M_V(cal) = 1.70$ for the assumed TYC2 color index $(B - V) = 0.40$.

3. SUMMARY

The paper presents radial-velocity data and orbital solutions for the sixth group of ten close binary systems that we observed at the David Dunlap Observatory. Only the detached, short-period system SV Cam was observed spectroscopically before. All systems except FS Leo are double-lined (SB2) binaries with visible spectral lines of both components and all, with the additional exception of SV Cam, are contact binaries.

Although our selection of our targets is quite unsystematic and is driven only by the brightness above the limit of about 11 mag. and the shortness of the orbital period (below one day), we continue seeing very interesting objects among the bright, photometrically discovered binaries. Eight of the systems are new photometric discoveries of the Hipparcos project. The magnitude-limited nature of the HIP survey has led to an emphasis on relatively luminous, massive, early-type (middle-A to early-F) contact systems. Because the Hipparcos mission discovered mostly small photometric amplitude systems, which were overlooked in previous whole-sky surveys, we tend to observe systems somewhat pre-selected in that they either have low orbital inclinations, such as V972 Her or ET Leo, or are members of triple systems as for KR Com, V401 Cyg, V2388 Oph and II UMa. In the latter case, while radial velocity amplitudes are large, the diminished photometric variation is due to the “dilution” of the variability signal in the combined light of the triple system. In addition to these four triple systems, we also observed separately a component in a wider visual binary, EE Cet; the other component of this system appears to be radial-velocity variable whose properties remain to be studied.

Support from the Natural Sciences and Engineering Council of Canada to SMR and SWM is acknowledged with gratitude.

The research has made use of the SIMBAD database, operated at the CDS, Strasbourg, France and accessible through the Canadian Astronomy Data Centre, which is operated by the Herzberg Institute of Astrophysics, National Research Council of Canada.

We thank the anonymous referee for the very careful and constructive review of the paper.

REFERENCES

Çiçek, C., Demircan, O., Erdem, A., Özdemir, S., Bulut, I., Soydugan, E., Soydugan, F. & Keskin, V. 2001, Inf. Bull. Var. Stars, 5144

European Space Agency. 1997. The Hipparcos and Tycho Catalogues (ESA SP-1200)(Noordwijk: ESA) (HIP)

Gomez–Forrellad, J. M., Garcia–Melendo, E., Guarro–Flo, J., Nomen–Torres, J. & Vidal–Saintz, J. 1999, Inf. Bull. Variable Stars, 4702

Herzeg, T. J. 1993, PASP, 105, 911

Hiltner, W. A. 1953, ApJ, 118, 262

Hoffmeister, C. 1929, Astr. Nachr., 236, 235

Hog, E., Fabricius, C., Makarov, V. V., Urban, S., Corbin, T., Wycoff, G., Bastian, U., Schwekendiek, P. & Wicenec, A. 2000, A&A, 355, L27 (TYC2)

Keskin, V., Yasarsoy, B. & Sipahi, E. 2000, Inf. Bull. Variable Stars, 4855

Lampens, P., Oblak, E., Duval, D. & Chareton, M. 2001, A&A, 374, 132

Lu, W., & Rucinski, S. M. 1999, AJ, 118, 515 (Paper I)

Lu, W., Rucinski, S. M. & Ogloza, W. 2001, AJ, 122, 402 (Paper IV)

Nelson, R. H. 2001, Inf. Bull. Variable Stars, 5040

Nordstroem, B., Stefanik, R. P., Latham, D. W., Andersen, J. 1997, A&AS, 126, 21

Oezeren, F. F., Gunn, A. G., Doyle, J. G. & Jevremovic, D. 2001, A&A, 366, 202

Patkos, L. & Hempelman, A. 1994, A&A, 292, 119

Pojmanski, G. 1998, Acta Astr., 48, 711

Pribulla, T., Vanko, M., Parimucha, S. & Chochol, D. 2001, Inf. Bull. Variable Stars, 5056

Rainger, P. P., Hilditch, R. W. & Edwin, R. P. 1991, MNRAS, 248, 168

Rodriguez, E. et al., 1998, A&A, 336, 920

Rucinski, S. M., & Duerbeck, H.W. 1997, PASP, 109, 1340 (RD97)

Rucinski, S. M. & Lu, W. 1999, AJ, 118, 2451 (Paper II)

Rucinski, S. M., Lu, W. & Mochnacki, S. W. 2000, AJ, 120, 1133 (Paper III)

Rucinski, S. M., Lu, W., Mochnacki, S. W., Ogloza, W. & Stachowski, G. 2001, AJ, 122, 1974 (Paper V)

Rucinski, S. M 2002, AJ, submitted (Paper VII)

Soederhjelm, S. 1999, A&A, 341, 121

Wolf, M., Molik, P., Hornoch, K. & Sarounova, L. 2000, A&AS, 147, 243

Yakut, K. & Ibanoglu, C. 2000, Inf. Bull. Variable Stars, 5002

This preprint was prepared with the AAS LaTeX macros v5.0.

Captions to figures:

Fig. 1.— Radial velocities of the systems SV Cam, EE Cet, KR Com and V401 Cyg are plotted in individual panels versus orbital phases. The lines give the respective circular-orbit (sine-curve) fits to the radial velocities. SV Cam is a close, detached binary. KR Com and V401 Cyg are A-type contact systems, while EE Cet is a W-type contact system. EE Cet, KR Com and V401 Cyg are members of triple systems although the companion of EE Cet could be excluded by the spectrograph slit. The circles and triangles in this and the next two figures correspond respectively to components eclipsed at the minimum corresponding to T_0 (as given in Table 2) or half a period later, while open symbols indicate observations contributing half-weight data in the solutions. Short marks in the lower parts of the panels show phases of available observations which were not used in the solutions because of the blending of lines. All panels have the same vertical ranges, -350 to $+350$ km s^{-1}.

Fig. 2.— Same as for Figure 1, but with the radial velocity orbits for the systems GM Dra, V972 Her, ET Leo and FS Leo. All systems, except FS Leo (which is a single-line binary of unknown type), are W-type contact systems.

Fig. 3.— Same as for Figure 1, for the systems V2388 Oph and II UMa. They are quite similar A-type contact systems with relatively long periods of slightly over 0.8 days, both being members of very close triple systems.

Fig. 4.— The broadening functions (BF's) for six close binary systems of this series. The two leftmost panels show the BF's for rather typical cases of a detached binary SV Cam and the contact binary GM Dra, both 9 magnitude objects. The spectroscopic triple systems are shown in the four center and right panels: The contact binary components result in broad BF's while the third body produces a narrow feature between the two broad components. Note the exceptionally well-defined BF's for the bright, 6 magnitude systems KR Com and V2388 Oph. All cases shown here illustrate orientations of components close to the orbital phase 0.25. The small third-body feature in the BF for V401 Cyg could be taken for a small error fluctuation if not for its persistence throughout all the phases.

Fig. 5.— The radial velocities of the companion of II UMa plotted versus the orbital phase of the close binary. In principle, there should be no relation between the two quantities, and thus we see here some sort of a "cross-talk". We have no explanation for the systematic trend in the deviations and, in particular, why the spread was larger for phases in the first half of the binary orbit. A similar, but smaller effect has been observed for V2388 Oph.

arXiv:astro-ph/0201213v2 29 May 2002

Table 1. DDO observations of the sixth group of ten close binary systems

HJD–2,400,000	Phase	V_1	ΔV_1	V_2	ΔV_2
SV Cam					
50730.6143	0.3832	−88.4	2.3	117.2	−1.0
50750.6585	0.1804	−122.5	−3.0	150.8	−12.4
50751.6033	0.7735	108.9	−2.5	−186.8	10.4
50751.8944	0.2643	−134.3	−3.8	189.1	8.8
50764.5407	0.5877	55.9	1.3	−123.2	−14.5
50764.5533	0.6089	66.8	−1.1	−135.0	−5.7
50756.6032	0.2040	−129.2	−3.3	165.6	−7.5
50756.6399	0.2659	−136.1	−5.7	179.1	−1.0
50756.6546	0.2907	−128.2	−1.2	174.7	−0.2
50756.6710	0.3183	−120.1	−0.2	164.9	1.1
50756.6863	0.3441	−108.4	1.9	164.6	15.8
50765.6861	0.5190	9.1	3.7	· · ·	· · ·
50765.6992	0.5411	25.1	3.1	· · ·	· · ·
50773.4635	0.6327	77.8	−3.3	−156.1	−6.2
50785.4480	0.8402	100.0	6.3	−169.0	0.6
50785.4622	0.8641	80.2	−2.5	−160.9	−8.4
50785.4772	0.8894	65.6	−3.3	−145.0	−14.1
50785.6032	0.1018	−84.8	−2.9	106.0	1.6
50785.6145	0.1209	−93.6	−0.5	123.1	1.3
50785.6274	0.1426	−105.3	−1.0	138.7	−0.7
50785.6388	0.1619	−108.1	4.7	160.1	7.5
50834.5804	0.6839	102.6	0.2	−184.0	−0.9
50834.5935	0.7060	107.5	−0.6	−187.3	4.8
50834.6444	0.7918	109.1	0.6	−186.4	6.4
50834.6591	0.8166	100.2	−2.0	−180.8	2.1
50834.6742	0.8421	89.3	−3.6	−174.8	−6.4
50850.6171	0.7239	113.6	2.5	−188.1	8.7
50850.6296	0.7450	114.9	2.2	−185.7	13.5
50854.4852	0.2461	−126.4	4.6	174.1	−6.9
50854.4970	0.2660	−125.0	5.4	184.9	4.8
EE Cet					
51781.8036	0.6185	185.0	2.5	−57.9	−2.6
51781.8132	0.6438	207.4	−3.8	−74.5	−10.1
51781.8228	0.6690	237.3	2.6	−76.6	−4.8
51781.8318	0.6927	243.2	−8.2	−80.3	−3.2
51781.8406	0.7159	253.4	−9.0	−86.0	−5.5
51781.8515	0.7446	269.9	1.5	−70.9	11.5
51781.8601	0.7672	264.6	−2.4	−81.0	1.0
51781.8686	0.7896	255.2	−5.1	−75.0	4.9
51781.8773	0.8125	256.4	8.2	−77.3	−1.2
51781.8860	0.8354	234.5	3.5	−65.9	4.7

Table 1—Continued

HJD–2,400,000	Phase	V_1	ΔV_1	V_2	ΔV_2
51781.8957	0.8609	219.7	13.4	−62.2	0.7
51781.9043	0.8835	199.4[a]	19.5	−54.6	−0.0
51785.7795	0.0837	...	...	...	...
51785.7911	0.1142	−202.6[a]	−28.7	53.2	−3.7
51785.8018	0.1424	−219.3	−12.7	61.5	−5.7
51785.8150	0.1771	−244.4	−6.6	81.5	4.5
51785.8256	0.2050	−255.7	−1.0	84.5	2.2
51806.7363	0.2452	−254.2	11.0	82.5	−3.1
51806.7470	0.2734	−262.2	0.2	77.6	−7.2
51806.7585	0.3036	−244.4	5.9	79.6	−1.3
51806.7681	0.3289	−229.5	3.7	81.3	5.8
51806.7788	0.3571	−201.5	5.7	76.2	8.9
51806.7883	0.3821	−182.2	−3.6	69.5	11.2
51855.6524	0.9999	...	...	...	...
51855.6634	0.0288	...	...	...	...
51855.6801	0.0728	...	...	...	...
51855.6923	0.1049	−180.2[a]	−18.3	49.0	−4.1
51855.7033	0.1339	−196.1	1.3	64.5	0.2
51855.7157	0.1665	−230.9	−1.5	71.7	−2.7
51855.7265	0.1949	−243.7	5.8	76.0	−4.7
KR Com					
51988.7208	0.8317	8.7	−0.1	−189.5	2.2
51988.7283	0.8503	7.2	−0.5	−182.5	−4.1
51988.7355	0.8678	8.2	1.9	−153.8[a]	10.0
51988.7457	0.8928	...	...	...	...
51988.7541	0.9135	...	...	...	...
51988.7617	0.9320	...	...	...	...
51988.7716	0.9562	...	...	...	...
51988.7788	0.9741	...	...	...	...
51988.7865	0.9929	...	...	...	...
51988.7941	0.0115	...	...	...	...
51988.8031	0.0336	...	...	...	...
51988.8106	0.0520	...	...	...	...
51988.8181	0.0702	...	...	...	...
51988.8273	0.0928	...	...	...	...
51988.8348	0.1113	−22.6	−2.4	...	...
51988.8424	0.1299	−18.4	3.4	146.4	0.5
51988.8512	0.1515	−24.7	−1.2	165.2	1.2
51988.8592	0.1710	−23.1	1.7	183.0	5.3
51988.8672	0.1906	−26.4	−0.7	184.7	−4.0
51988.8819	0.2266	−28.9	−2.0	194.0	−6.9
51991.7656	0.2951	−27.7	−1.4	194.0	−0.8

Table 1—Continued

HJD–2,400,000	Phase	V$_1$	ΔV$_1$	V$_2$	ΔV$_2$
51991.7767	0.3223	−28.5	−3.4	182.2	0.4
51991.7886	0.3515	−23.1	0.2	174.5[a]	12.8
51991.7992	0.3776	···	···	···	···
51991.8131	0.4116	···	···	···	···
51991.8234	0.4368	···	···	···	···
51991.8359	0.4674	···	···	···	···
51991.8469	0.4943	···	···	···	···
51991.8587	0.5233	···	···	···	···
51991.8694	0.5496	···	···	···	···
51991.8812	0.5786	···	···	···	···
51991.8919	0.6046	···	···	···	···
51991.9048	0.6364	2.4[a]	−4.3	−167.2	0.2
51991.9156	0.6628	5.9	−2.6	−187.5	0.5
52002.7182	0.1418	−22.0	0.8	155.3	−1.0
52002.7276	0.1649	−23.1	1.2	179.2	5.5
52002.7412	0.1982	−25.2	0.8	191.0	−1.1
52002.7537	0.2290	−25.7	1.2	201.4	0.1
52002.7668	0.2609	−27.4	−0.4	205.7	3.0
52002.7775	0.2871	−28.6	−2.0	201.1	3.6
52014.7539	0.6433	0.9[a]	−6.2	−194.5[a]	−21.2
52014.7626	0.6647	5.1	−3.5	−196.1	−6.8
52014.7713	0.6861	9.7	−0.0	−199.4	2.8
52014.7812	0.7104	9.9	−0.8	−209.2	3.2
52014.7898	0.7314	11.2	−0.0	−213.6	3.9
52014.7981	0.7518	12.1	0.8	−213.8	5.1
52014.8091	0.7788	12.4	1.4	−214.0	1.5
52014.8183	0.8013	12.6	2.2	−208.7	−0.6
52014.8286	0.8264	9.1	−0.1	−199.6	−4.5
52014.8385	0.8508	5.7	−1.9	−176.1	1.9
52014.8493	0.8771	3.6[a]	−1.9	−169.6[a]	−14.5
52014.8603	0.9042	···	···	···	···
52014.8727	0.9346	···	···	···	···
52014.8840	0.9623	···	···	···	···
52014.8965	0.9929	···	···	···	···
52014.9053	0.0145	···	···	···	···
V401 Cyg					
51479.4731	0.0528	−12.5	−14.4	···	···
51479.4853	0.0739	−14.8	−8.0	···	···
51479.4989	0.0972	−27.8	−11.9	177.6[a]	9.2
51479.5119	0.1194	−31.9	−8.1	217.6[a]	22.2
51479.5287	0.1482	−46.3	−13.9	224.1	−1.4
51479.5430	0.1729	−48.7	−10.3	245.1	−0.8

Table 1—Continued

HJD–2,400,000	Phase	V_1	ΔV_1	V_2	ΔV_2
51479.5584	0.1992	−51.4	−8.3	277.0	14.9
51479.5727	0.2239	−48.8	−3.0	273.1	1.8
51479.5894	0.2525	−46.6	0.1	275.8	1.2
51479.6035	0.2767	−46.1	−0.4	254.8	−16.3
51479.6206	0.3061	−47.0	−4.7	240.2	−19.1
51479.6357	0.3319	−36.4	1.0	250.4	8.0
51659.8316	0.5676	43.5	−11.7	···	···
51659.8552	0.6080	63.0	−7.9	−179.1[a]	−48.3
51659.8784	0.6477	64.8	−18.6	−191.8[a]	−17.9
51663.8205	0.4129	−23.1	−11.0	212.6[a]	57.4
51663.8388	0.4443	0.7	−0.1	···	···
51663.8544	0.4710	12.1	−0.4	···	···
51663.8711	0.4997	2.0	−23.4	···	···
51723.6135	0.0241	10.1	−4.5	···	···
51723.6250	0.0439	1.3[a]	−4.6	···	···
51723.6389	0.0678	−15.7[a]	−11.4	198.5[a]	70.0
51723.6497	0.0862	−21.9	−10.2	199.4[a]	45.5
51723.6621	0.1075	−34.1	−14.4	203.2	21.9
51723.6735	0.1270	−25.3	0.9	242.0	38.1
51723.6880	0.1520	−39.9	−6.5	245.9	17.0
51723.6998	0.1722	−40.6	−2.4	226.1	−19.4
51723.7119	0.1930	−40.3[a]	1.9	266.8[a]	7.9
51723.7229	0.2119	−37.8[a]	6.9	242.0[a]	−25.6
51723.7381	0.2380	−42.1[a]	4.4	271.9[a]	−2.0
51723.7489	0.2566	−48.6[a]	−2.0	···	···
51723.7613	0.2778	−42.7[a]	2.9	233.9[a]	−37.0
51723.7722	0.2964	−44.5[a]	−0.8	233.7[a]	−30.4
51723.7850	0.3184	−40.2[a]	−0.1	267.5[a]	15.5
51723.7958	0.3369	−44.8	−8.6	229.4	−9.1
51723.8117	0.3642	−23.2	5.6	240.7	27.5
51723.8250	0.3870	−26.9	−5.3	241.1	53.2
51723.8383	0.4100	−6.8	6.3	234.2[a]	75.1
51764.7805	0.6712	80.1	−8.9	−161.8	31.9
51764.7945	0.6952	69.4	−24.1	−176.1[a]	32.9
51781.6617	0.6410	60.3[a]	−21.2	−184.8[a]	−17.3
51781.6758	0.6653	78.0[a]	−9.8	−178.6[a]	10.5
51781.6938	0.6961	105.1	11.4	−193.2	16.2
51781.7082	0.7208	90.4	−6.1	−198.0	21.4
51781.7235	0.7471	92.1	−5.7	−198.0	25.5
51781.7379	0.7718	91.6	−5.4	−234.0	−12.8
51781.7545	0.8004	86.0	−8.2	−193.7	17.5
51781.7688	0.8248	78.8	−11.1	−194.2	2.4

Table 1—Continued

HJD–2,400,000	Phase	V_1	ΔV_1	V_2	ΔV_2
GM Dra					
51039.5709	0.5733	···	···	···	···
51039.5782	0.5949	···	···	···	···
51039.5856	0.6167	···	···	···	···
51039.5938	0.6409	−36.3	−9.3	216.5	7.1
51039.6011	0.6625	−37.3	−6.6	244.5	14.8
51039.6084	0.6840	−35.2	−1.6	256.2	10.3
51039.6175	0.7109	−38.9	−2.7	271.1	11.0
51039.6251	0.7333	−40.1	−2.8	263.7	−2.7
51039.6331	0.7569	−41.5	−4.0	275.2	7.6
51039.6420	0.7832	−33.1	3.5	259.1	−3.1
51039.6501	0.8071	−54.6	−20.0	256.5	5.1
51039.6580	0.8304	−25.8	5.9	198.8	−36.7
51039.6677	0.8591	−38.0	−11.0	205.2	−4.2
51039.6760	0.8836	−17.0	5.1	162.9	−19.0
51039.6846	0.9090	−53.4	−37.2	···	···
51074.6828	0.2271	46.6	−8.7	−252.1	−5.2
51074.6910	0.2513	45.5	−10.3	−254.8	−5.2
51074.6982	0.2726	53.6	−1.7	−242.8	4.2
51074.7062	0.2962	46.1	−7.8	−257.5	−18.7
51074.7134	0.3175	55.4	3.7	−214.0	12.7
51074.7207	0.3390	43.8	−4.9	−203.6	6.6
51075.5244	0.7116	−31.8	4.4	262.4	2.0
51075.5313	0.7320	−33.9	3.4	278.7	12.5
51075.5389	0.7544	−41.6	−4.0	269.1	1.4
51075.5490	0.7842	−25.1	11.4	273.6	11.7
51075.5561	0.8052	−35.0	−0.2	258.2	5.8
51075.5633	0.8264	−28.9	3.4	242.5	3.9
51297.8288	0.9763	···	···	···	···
51297.8358	0.9969	···	···	···	···
51326.7576	0.3769	43.5	1.8	−179.0	−7.4
51326.7649	0.3985	58.6	21.7	−112.1	32.8
51326.7731	0.4227	···	···	···	···
51326.7804	0.4443	···	···	···	···
51326.7895	0.4711	···	···	···	···
51326.7969	0.4930	···	···	···	···
51326.8038	0.5133	···	···	···	···
51648.8182	0.1318	47.5	4.0	−148.9	32.6
51648.8260	0.1548	37.4	−10.3	−206.3	−1.6
51648.8338	0.1779	43.5	−7.6	−211.7	11.8
51649.7779	0.9649	···	···	···	···
51649.7865	0.9903	···	···	···	···

Table 1—Continued

HJD–2,400,000	Phase	V_1	ΔV_1	V_2	ΔV_2
51649.7950	0.0154	···	···	···	···
51649.8054	0.0461	···	···	···	···
51649.8139	0.0712	···	···	···	···
51649.8225	0.0966	···	···	···	···
51649.8330	0.1276	38.0	−4.7	−160.5	16.3
51649.8415	0.1527	38.9	−8.5	−207.6	−4.9
51660.5708	0.8266	−37.0	−4.7	251.2	12.8
51660.5958	0.9004	−32.3	−14.1	176.0	15.4
51660.6081	0.9368	···	···	···	···
51660.6206	0.9737	···	···	···	···
51660.6327	0.0094	···	···	···	···
51660.6463	0.0495	···	···	···	···
51660.6586	0.0858	···	···	···	···
51660.6707	0.1216	29.5	−11.9	−163.3	6.5
51660.6824	0.1561	37.9	−10.0	−205.5	0.4
V972 Her					
51039.7155	0.5807	···	···	···	···
51039.7271	0.6069	···	···	···	···
51039.7407	0.6376	119.1[a]	−3.3	−18.7	−2.9
51039.7491	0.6566	126.9	−6.7	−22.4	−4.8
51039.7566	0.6735	143.0	1.0	−19.6	−0.6
51039.7645	0.6913	150.3	1.1	−19.6	0.6
51039.7739	0.7125	151.0	−4.3	−22.8	−1.5
51039.7815	0.7297	152.9	−5.5	−23.9	−2.1
51039.7888	0.7462	153.2	−6.4	−24.1	−2.1
51065.6043	0.0081	···	···	···	···
51065.6126	0.0268	···	···	···	···
51065.6207	0.0451	···	···	···	···
51065.6319	0.0704	···	···	···	···
51065.6400	0.0886	···	···	···	···
51065.6477	0.1060	···	···	16.7	−3.3
51065.6578	0.1288	−122.3[a]	−13.6	20.4	−2.4
51065.6749	0.1674	−144.0	−12.8	25.9	−0.6
51065.6832	0.1861	−148.5	−9.2	28.3	0.4
51065.6941	0.2107	−150.5	−3.5	28.5	−0.6
51065.7020	0.2286	−153.1	−2.8	27.6	−2.1
51065.7093	0.2450	−149.6	2.0	29.7	−0.2
51065.7190	0.2669	−151.1	−0.3	29.6	−0.2
51065.7268	0.2845	−146.0	2.0	26.9	−2.4
51074.5801	0.2652	−149.6	1.4	31.8	2.0
51074.5858	0.2780	−145.7	3.6	31.6	2.1
51074.5917	0.2914	−144.0	2.5	28.9	−0.2

Table 1—Continued

HJD–2,400,000	Phase	V_1	ΔV_1	V_2	ΔV_2
51074.5976	0.3047	−139.5	3.1	29.3	0.9
51074.6044	0.3200	−134.0	2.9	28.8	1.3
51074.6102	0.3331	−128.7	2.2	29.4	2.9
51074.6160	0.3462	−120.5	3.6	26.9	1.6
51074.6218	0.3593	−111.6[a]	4.8	25.6	1.6
51074.6296	0.3769	···	···	19.6	−2.5
51074.6355	0.3902	···	···	17.8	−2.7
51074.6417	0.4042	···	···	···	···
51075.5772	0.5155	···	···	···	···
51075.5848	0.5326	···	···	···	···
51075.5920	0.5489	···	···	···	···
51075.6004	0.5678	···	···	···	···
51075.6079	0.5848	···	···	···	···
51075.6154	0.6017	···	···	···	···
51075.6244	0.6220	···	···	−18.9	−4.9
51075.6316	0.6383	121.3[a]	−1.5	−17.3	−1.5
51082.5488	0.2494	−151.5	0.2	32.7	2.8
51082.5562	0.2661	−147.5	3.4	29.0	−0.8
51082.5636	0.2828	−147.1	1.3	28.4	−1.0
51284.7545	0.5988	···	···	···	···
51284.7604	0.6122	···	···	···	···
51284.7663	0.6255	···	···	−14.9	−0.5
51657.7893	0.4852	···	···	···	···
51659.6846	0.7626	155.1	−4.0	−21.6	0.3
51659.6900	0.7748	154.8	−2.9	−21.6	0.1
51659.6949	0.7859	151.7	−4.0	−21.7	−0.4
51659.6998	0.7969	152.6	−0.3	−17.9	3.0
51659.7071	0.8134	150.2	2.8	−19.5	0.4
51659.7120	0.8245	146.3	3.4	−19.7	−0.5
51659.7169	0.8355	145.0	7.3	−17.0	1.3
51659.7218	0.8466	139.8	8.0	−16.7	0.6
51659.7294	0.8637	133.7	12.2	−13.0	2.6
51659.7343	0.8748	130.1[a]	15.9	−10.4	4.0
51659.7392	0.8859	···	···	−9.3	3.8
51659.7441	0.8969	···	···	−4.7	7.0
51659.7524	0.9156	···	···	···	···
51659.7573	0.9267	···	···	···	···
51659.7622	0.9378	···	···	···	···
51659.7671	0.9488	···	···	···	···
51659.7791	0.9759	···	···	···	···
51659.7848	0.9888	···	···	···	···
51659.7897	0.9998	···	···	···	···

Table 1—Continued

HJD–2,400,000	Phase	V_1	ΔV_1	V_2	ΔV_2
51659.7972	0.0168	···	···	···	···
51659.8021	0.0278	···	···	···	···
51659.8070	0.0389	···	···	···	···
51659.8119	0.0499	···	···	···	···
ET Leo					
51907.8761	0.1314	−111.1	−5.4	54.3	−10.6
51907.8869	0.1627	−124.3	1.8	69.0	−2.9
51918.7431	0.4934	···	···	···	···
51947.7226	0.1276	−97.8[a]	5.0	63.0[a]	−0.9
51954.6350	0.0767	···	···	···	···
51954.6422	0.0974	···	···	···	···
51954.6493	0.1180	−100.3[a]	−5.0	53.6[a]	−7.8
51954.6595	0.1474	−116.2	0.5	65.5	−3.2
51954.6665	0.1675	−130.7	−1.9	65.3	−7.5
51956.6717	0.9546	···	···	···	···
51956.6826	0.9858	···	···	···	···
51959.8832	0.2228	−153.6	−4.6	77.3	−2.3
51959.8929	0.2507	−155.2	−3.7	77.7	−2.8
51959.9066	0.2903	−152.8	−6.8	77.0	−1.6
51961.6328	0.2722	−149.0	0.8	80.5	0.6
51961.6403	0.2937	−143.4	1.7	79.5	1.2
51961.6475	0.3144	−141.8	−4.3	77.0	1.2
51961.6550	0.3363	−130.2	−3.5	74.0	1.9
51961.6621	0.3566	−117.4	−3.3	72.0	4.3
51968.6542	0.5357	···	···	···	···
51968.6613	0.5563	···	···	···	···
51968.6687	0.5774	···	···	···	···
51968.6797	0.6092	118.8[a]	−12.3	−24.0[a]	−8.1
51968.6873	0.6312	151.3[a]	2.9	−19.2[a]	2.7
51968.6948	0.6527	165.2	2.1	−25.5	1.5
51968.7051	0.6826	177.1	−2.0	−36.9	−4.6
51968.7125	0.7039	184.8	−2.4	−39.8	−4.6
51968.7203	0.7263	186.2	−6.3	−36.4	0.6
51968.7301	0.7548	190.0	−4.3	−35.3	2.3
51968.7373	0.7755	188.9	−3.3	−45.5	−8.7
51968.7447	0.7969	190.4	3.4	−35.8	−0.7
51968.7549	0.8263	182.6	7.7	−33.0	−2.0
51968.7623	0.8476	177.4	14.5	−24.0	2.8
51968.7696	0.8687	152.3[a]	3.8	−23.9[a]	−2.0
51968.7791	0.8961	139.6[a]	13.0	−16.4[a]	−2.0
51968.7996	0.9552	···	···	···	···
51968.8068	0.9761	···	···	···	···

Table 1—Continued

HJD–2,400,000	Phase	V_1	ΔV_1	V_2	ΔV_2
51968.8143	0.9977	⋯	⋯	⋯	⋯
51968.8233	0.0236	⋯	⋯	⋯	⋯
51968.8306	0.0448	⋯	⋯	⋯	⋯
51968.8374	0.0643	⋯	⋯	⋯	⋯
51989.6276	0.0645	⋯	⋯	⋯	⋯
51989.6383	0.0953	⋯	⋯	⋯	⋯
51989.6506	0.1308	−104.2[a]	1.0	60.0[a]	−4.7
51989.6617	0.1628	−123.8	2.4	68.7	−3.2
51989.6779	0.2097	−144.6	1.4	76.0	−2.7
51989.6889	0.2413	−154.3	−3.1	78.8	−1.6
51989.7025	0.2806	−139.3	9.0	79.7	0.2
51989.7144	0.3150	−135.6	1.7	78.7	3.1
51989.7265	0.3498	−122.1	−3.5	70.2	0.9
51989.7391	0.3863	−88.8[a]	3.1	63.8[a]	3.6
51989.7496	0.4166	−38.3	26.8	⋯	⋯
52073.5849	0.3635	−95.2	14.1	77.2	11.0
52073.5961	0.3957	⋯	⋯	⋯	⋯
52073.6088	0.4324	⋯	⋯	⋯	⋯
52073.6224	0.4715	⋯	⋯	⋯	⋯
FS Leo					
51907.8239	0.7264	22.3	0.1		
51907.8345	0.7496	23.7	0.9		
51907.8484	0.7801	17.5	−4.4		
51907.8598	0.8051	19.4	−0.2		
51975.6796	0.2167	−79.4	3.8		
51975.6902	0.2399	−88.0	−3.8		
51975.7037	0.2694	−82.1	1.9		
51975.7151	0.2943	−80.5	1.8		
51975.7271	0.3206	−84.3	−5.1		
51975.7381	0.3446	−74.0	1.1		
51984.6316	0.8064	23.1	3.5		
51984.6442	0.8341	18.3	2.7		
51984.6573	0.8627	14.2	4.2		
51984.6698	0.8901	1.7	−1.7		
51984.7016	0.9596	−6.9	10.4		
51984.7136	0.9858	−19.8	6.2		
51984.7258	0.0126	−36.5	−1.6		
51984.7384	0.0401	−52.9	−8.7		
51984.7508	0.0673	−53.7	−0.9		
51984.7636	0.0954	−65.4	−4.4		
52013.5549	0.0999	−65.5	−3.3		
52013.5657	0.1237	−72.4	−4.1		

Table 1—Continued

HJD–2,400,000	Phase	V_1	ΔV_1	V_2	ΔV_2
52013.5775	0.1494	−77.6	−3.7		
52013.5881	0.1726	−80.3	−2.2		
52013.6002	0.1992	−80.0	1.6		
52013.6110	0.2228	−81.6	1.9		
52013.6271	0.2580	−84.3	0.0		
52013.6388	0.2835	−78.0	5.2		
52013.6506	0.3094	−79.4	1.3		
52013.6614	0.3331	−74.8	2.4		
52013.6746	0.3618	−69.9	1.8		
52013.6853	0.3853	−60.9	5.2		
52013.6977	0.4124	−60.5	−1.7		
52013.7087	0.4366	−51.9	−0.4		
52013.7214	0.4643	−41.3	1.4		
52013.7337	0.4912	−34.5	−0.8		
52013.7446	0.5152	−25.6	0.1		
52013.7583	0.5451	−15.4	0.4		
52013.7700	0.5708	−9.6	−1.9		
52013.7822	0.5973	−4.0	−4.0		
52013.7935	0.6221	1.3	−5.1		
V2388 Oph					
51374.5934	0.8058	16.5	0.5	−249.0	2.5
51374.6008	0.8150	17.2	2.1	−241.0	5.3
51374.6080	0.8240	15.3	1.3	−238.1	2.5
51374.6170	0.8352	···	···	···	···
51374.6242	0.8442	14.5	3.4	−234.6	−9.4
51374.6318	0.8537	15.3	5.7	−221.9	−5.0
51374.6403	0.8643	14.2	6.5	−212.8	−6.0
51374.6481	0.8740	11.9	6.0	−203.0	−6.2
51374.6558	0.8836	14.0	10.1	−184.9	1.4
51374.6650	0.8951	11.7	10.3	−176.3	−3.3
51374.6725	0.9044	8.7	9.4	−165.3	−3.7
51374.7151	0.9575	···	···	···	···
51374.7226	0.9669	···	···	···	···
51374.7302	0.9763	···	···	···	···
51379.7849	0.2766	−66.8	3.1	208.3	−2.7
51379.7921	0.2856	−65.5	3.9	209.4	1.1
51379.7993	0.2946	−67.2	1.6	204.1	−0.9
51379.8075	0.3048	−64.4	3.5	201.6	1.4
51379.8146	0.3136	−64.5	2.5	200.9	5.5
51381.6340	0.5814	−7.5	−3.4	···	···
51381.6409	0.5900	−5.1	−3.1	−171.0[a]	−16.4
51381.6458	0.5961	−2.7	−2.1	−175.2[a]	−13.0

Table 1—Continued

HJD–2,400,000	Phase	V_1	ΔV_1	V_2	ΔV_2
51381.6536	0.6058	−1.9	−3.5	−186.9	−12.8
51381.6609	0.6149	1.1	−2.5	−194.8	−10.2
51381.6681	0.6239	2.6	−2.8	−201.7	−7.2
51381.6763	0.6341	4.3	−3.1	−214.9	−9.7
51381.6842	0.6439	7.3	−1.9	−217.2	−2.5
51381.6917	0.6533	11.1	0.4	−227.9	−4.8
51381.7037	0.6682	13.7	0.7	−237.3	−2.2
51381.7115	0.6780	13.6	−0.6	−238.7	3.2
51381.7193	0.6877	12.2	−3.2	−248.4	−0.5
51381.7282	0.6988	14.3	−2.1	−252.4	1.4
51381.7387	0.7119	17.2	−0.3	−255.5	3.7
51381.7461	0.7211	14.8	−3.2	−259.5	2.6
51381.7554	0.7327	18.6	0.1	−260.7	4.0
51381.7633	0.7425	18.3	−0.4	−258.3	7.5
51381.7716	0.7529	19.1	0.4	−262.6	3.5
51381.7805	0.7640	20.3	1.7	−258.6	6.6
51381.7882	0.7736	19.0	0.8	−260.9	2.6
51409.5652	0.3954	−51.1	2.1	148.2[a]	27.3
51409.5725	0.4045	−48.4	2.7	147.6[a]	37.8
51409.5797	0.4134	−46.8	2.2	· · ·	· · ·
51409.5888	0.4248	−43.9	2.3	· · ·	· · ·
51409.5960	0.4337	−41.6	2.3	· · ·	· · ·
51409.6032	0.4427	−41.1	0.5	· · ·	· · ·
51409.6137	0.4558	· · ·	· · ·	· · ·	· · ·
51409.6209	0.4648	· · ·	· · ·	· · ·	· · ·
51409.6281	0.4738	· · ·	· · ·	· · ·	· · ·
51663.7023	0.1568	−63.2	−0.1	173.3	−1.0
51663.7092	0.1654	−64.9	−0.5	175.6	−5.6
51663.7188	0.1774	−66.0	−0.1	186.6	−3.2
51663.7254	0.1856	−68.4	−1.5	187.8	−7.1
51663.7499	0.2162	−69.8	−0.3	202.6	−6.3
51663.7561	0.2239	−69.1	0.8	202.5	−8.6
51663.7801	0.2538	−70.5	−0.0	206.4	−7.9
51663.7877	0.2633	−71.0	−0.6	208.6	−4.9
51764.7337	0.0844	−51.2	−2.8	· · ·	· · ·
51764.7411	0.0936	−51.3	−0.7	114.8[a]	7.4
51764.7484	0.1027	−52.7	0.0	125.1	6.5
51764.7566	0.1129	−52.6	2.4	136.6	6.0
51764.7641	0.1223	−56.8	0.1	142.3	1.3
II UMa					
50853.8300	0.2670	−47.2	3.8	230.8	−10.7
50853.8376	0.2761	−44.5	6.1	233.4	−6.2

Table 1—Continued

HJD–2,400,000	Phase	V_1	ΔV_1	V_2	ΔV_2
50853.8457	0.2860	−44.9	5.2	234.0	−2.5
50853.8565	0.2991	−42.8	6.4	227.3	−3.8
50853.8640	0.3082	−43.3	5.1	224.7	−1.7
50853.8712	0.3169	−44.1	3.3	214.2	−6.9
50858.7464	0.2246	−47.0	3.6	242.3[a]	2.6
50858.7536	0.2334	−48.1	2.9	215.5[a]	−26.1
50858.7609	0.2422	−47.7	3.4	233.9	−8.8
50858.7703	0.2536	−44.5	6.7	237.9	−5.0
50858.7775	0.2624	−46.0	5.0	239.8	−2.4
50858.7847	0.2711	−45.7	5.1	213.2[a]	−27.6
50858.7937	0.2820	−45.9	4.4	228.5	−9.4
50858.8012	0.2910	−47.8	2.0	224.2	−10.4
50858.8085	0.2999	−46.7	2.3	227.9	−2.8
50860.7344	0.6336	29.9	5.8	−231.1	−36.2
50860.7458	0.6475	30.2	3.7	−238.0	−29.2
50860.7741	0.6818	30.8	−0.5	−250.7	−14.4
50860.8154	0.7319	36.4	1.6	−259.8	−2.4
50860.8440	0.7665	37.6	2.7	−248.4	9.3
50860.8692	0.7971	41.1	7.8	−242.8	5.3
50860.9028	0.8377	36.9	8.1	−231.3	−9.5
50860.9102	0.8467	31.0	3.6	−220.2[a]	−6.1
50860.9174	0.8555	35.3	9.3	−214.7[a]	−8.9
50860.9383	0.8808	23.5	2.1	−215.7[a]	−36.8
50860.9457	0.8897	22.0	2.4	−215.6[a]	−47.2
50860.9530	0.8986	21.5	3.9	−215.6[a]	−58.2
50860.9613	0.9086	20.9	5.5	· · ·	· · ·
50860.9691	0.9181	20.0	6.8	· · ·	· · ·
50860.9768	0.9275	20.0	9.0	· · ·	· · ·
50896.8361	0.3817	−30.7	6.5	182.3[a]	20.5
50896.8448	0.3922	−31.4	3.7	182.4[a]	33.2
50930.6715	0.3833	−34.1	2.8	182.3[a]	22.3
50930.6801	0.3937	−31.7	3.0	181.0[a]	33.6
50930.6910	0.4070	−24.2	7.6	· · ·	· · ·
50930.7007	0.4187	−17.8	11.3	· · ·	· · ·
50939.5985	0.2011	−45.5	3.7	219.0[a]	−12.2
50940.6306	0.4518	−10.2	10.7	· · ·	· · ·
50940.7619	0.6109	15.8	−3.9	−239.7[a]	−70.6
50941.6507	0.6879	29.4	−2.5	−252.0	−11.8
50941.6614	0.7008	37.0	3.9	−248.3	−1.2
50941.6739	0.7161	39.3	5.1	−246.4	6.9
50941.6846	0.7290	40.9	6.2	−267.2	−10.4
50941.6976	0.7448	34.1	−1.0	−255.2	3.6

Table 1—Continued

HJD–2,400,000	Phase	V_1	ΔV_1	V_2	ΔV_2
50941.7095	0.7592	32.7	−2.4	−261.2	−2.6
50941.7229	0.7754	25.1[a]	−9.5	−267.8[a]	−12.0
50941.7343	0.7892	48.3	14.5	−211.6	39.8
50960.7181	0.7938	33.2	−0.3	−253.1	−3.6
50960.7340	0.8131	36.7	4.9	−239.8	−0.3
51284.6349	0.3155	−44.8	2.7	230.7	8.7
51284.6455	0.3284	−46.7	−0.7	214.0	0.9
51284.6583	0.3438	−46.1	−2.2	206.0	5.4
51284.6689	0.3568	−41.6	0.2	205.8	17.3
51589.7831	0.0936	−38.1[a]	−6.2	···	···
51589.7994	0.1132	−38.6[a]	−2.4	···	···
51589.8154	0.1327	−46.5	−6.5	171.8[a]	−6.0
51589.8313	0.1519	−50.8	−7.6	187.4	−9.4
51589.8479	0.1721	−48.2[a]	−2.1	197.1[a]	−16.4
51589.8642	0.1918	−53.8	−5.5	196.7	−29.7
51589.8785	0.2091	−48.7	1.0	238.8[a]	4.1

[a] These data have been given half weight in the orbital solution.

Note. — Velocities are expressed in km s^{-1}. The deviations ΔV_i are relative to the simple sine-curve fits to the radial velocity data. Observations leading to entirely unseparable broadening- and correlation-function peaks are marked by the "no-data" symbol (···); these observations may be eventually used in more extensive modeling of broadening functions. The radial velocities designated as V_1 correspond to the component eclipsed during the primary minimum at the epoch given as T_0 in Table 2.

arXiv:astro-ph/0201213v2 29 May 2002

Table 2. Spectroscopic orbital elements of the sixth set of ten close binary systems

Name	Type	Other names	V_0	K_1	ϵ_1	T_0 – 2,400,000	P (days)	q
	Sp. type			K_2	ϵ_2	(O–C)(d) [E]	$(M_1+M_2)\sin^3 i$	
SV Cam	EA/RS	HD 44982	−9.13(0.78)	121.86(0.76)	3.10	50,792.6597(11)	0.593073	0.641(7)
	G2V	HIP 32015		190.17(1.73)	7.79	+0.0012 [0]	1.871(45)	
EE Cet	EW/W	HD 17613	+1.60(0.93)	84.05(1.24)	5.43	51,818.8005(7)	0.379917	0.315(5)
ADS 2163(S)	F8V	HIP 13199		266.92(1.54)	8.32	+0.0315 [8735]	1.706(41)	
KR Com	EW/A	HD 115955	−7.86(0.38)	19.18(0.34)	1.85	52,001.4365(4)	0.407968	0.091(2)
ADS 8863A	G0IV	HIP 65069		211.07(0.80)	4.45	+0.0430 [8582]	0.517(8)	
V401 Cyg	EW/A	BD+30°3592	+25.53(2.14)	72.23(2.43)	9.74	51,630.9481(35)	0.582714	0.290(11)
	F0V	HIP 95816		249.13(4.53)	26.87	−0.0047 [−192]	2.008(130)	
GM Dra	EW/W	HD 238677	+9.12(1.63)	46.69(1.74)	10.45	51,350.3418(13)	0.338741	0.180(7)
	F5V	HIP 84837		258.72(2.66)	13.69	−0.0058 [−1181]	1.002(42)	
V972 Her	EW/W	HD 164078	+3.98(0.46)	25.95(0.36)	2.34	51,349.1808(16)	0.443094	0.167(3)
	F4V	HIP 87958		155.65(1.00)	5.51	+0.0224 [6430]	0.276(6)	
ET Leo	EW/W	HD 91386	+21.46(0.78)	59.08(0.80)	4.36	51,990.9912(13)	0.346503	0.342(5)
	G8V	HIP 51677		172.95(1.20)	7.30	+0.0021 [10075]	0.450(12)	
FS Leo	EB?	BD+15°2335	−30.75(0.64)	53.60(0.74)	3.62	51,660.2706(14)	0.456971	
	F2V	HIP 55952				−0.0349 [6915]		
V2388 Oph	EW/A	HD 163151	−25.88(0.52)	44.62(0.48)	3.36	51,569.7076(12)	0.802298	0.186(2)
Fin 381A	F3V	HIP 87655		240.22(0.98)	7.59	−0.0108 [2093]	1.926(30)	
II UMa	EW/A	HD 109247	−8.02(1.10)	43.16(0.86)	5.46	51,221.6579(44)	0.825220	0.172(4)
ADS 8594A	F5III	HIP 61237		250.96(2.74)	18.64	−0.0007 [3298]	2.180(80)	

[a] SV Cam: T_0 has been advanced from the published time to the time of observations.

Note. — The spectral types given in column two are all new and relate to the combined spectral type of all components in a system. The convention of naming the binary components is that the subscript 1 designates the component which is more massive so that the mass ratio is defined to be always $q \leq 1$. The standard errors of the circular solutions in the table are expressed in units of last decimal places quoted; they are given in parantheses after each value. For example, the last table entry for the mass ratio q, 0.172(4), should be interpretted as $q = 0.172 \pm 0.004$. The center-of-mass velocities (V_0), the velocity amplitudes (K_i) and the standard unit-weight errors of the solutions (ϵ) are all expressed in km s^{-1}. The spectroscopically determined moments of primary minima are given by T_0; the corresponding (O–C) deviations (in days) have been calculated from the most recent available ephemerides, as given in the text, using the assumed periods and the number of epochs given by [E]. The values of $(M_1 + M_2)\sin^3 i$ are in the solar mass units.